AGU PUBLICATIONS

Global Biogeochemical Cycles

RESEARCH ARTICLE
10.1002/2017GB005637

Key Points:
- The characteristics of surface water DMS and pCO_2 distributions from the Southern Ocean to northwest Pacific Ocean are investigated
- The correlations between DMS, pCO_2, and environmental parameters are analyzed
- Anticorrelation between DMS and pCO_2 is found in the seasonal ice zone of the Southern Ocean

Supporting Information:
- Supporting Information S1
- Data Set S1
- Data Set S2

Correspondence to:
M. Zhang and L. Chen,
zhangmiming@tio.org.cn;
liqichen@tio.org.cn

Citation:
Zhang, M., et al. (2017), Characteristics of the surface water DMS and pCO_2 distributions and their relationships in the Southern Ocean, southeast Indian Ocean, and northwest Pacific Ocean, *Global Biogeochem. Cycles*, *31*, 1318–1331, doi:10.1002/2017GB005637.

Received 8 FEB 2017
Accepted 6 AUG 2017
Accepted article online 11 AUG 2017
Published online 26 AUG 2017

Characteristics of the surface water DMS and pCO_2 distributions and their relationships in the Southern Ocean, southeast Indian Ocean, and northwest Pacific Ocean

Miming Zhang[1], C. A. Marandino[2], Liqi Chen[1], Heng Sun[1], Zhongyong Gao[1], Keyhong Park[3], Intae Kim[4], Bo Yang[5], Tingting Zhu[6], Jinpei Yan[1], and Jianjun Wang[1]

[1]Key Laboratory of Global change and Marine-Atmospheric Chemistry, Third Institute of Oceanography, State Oceanic Administration, Xiamen, China, [2]Forschungsberech Marine Biogeochemie, GEOMAR Helmholtz-Zentrum für Ozeanforschung Kiel, Germany, [3]Division of Polar Ocean Science, Korea Polar Research Institute, Incheon, South Korea, [4]Marine Radionuclide Research Center, Korea Institute of Ocean Science and Technology, Ansan, South Korea, [5]School of Oceanography, University of Washington, Seattle, Washington, USA, [6]State Key laboratory of Information Engineering in Surveying, Mapping and Remote Sensing (LIESMARS), Wuhan University, Wuhan, China

Abstract Oceanic dimethyl sulfide (DMS) is of interest due to its critical influence on atmospheric sulfur compounds in the marine atmosphere and its hypothesized significant role in global climate. High-resolution shipboard underway measurements of surface seawater DMS and the partial pressure of carbon dioxide (pCO_2) were conducted in the Atlantic Ocean and Indian Ocean sectors of the Southern Ocean (SO), the southeast Indian Ocean, and the northwest Pacific Ocean from February to April 2014 during the 30th Chinese Antarctic Research Expedition. The SO, particularly in the region south of 58°S, had the highest mean surface seawater DMS concentration of 4.1 ± 8.3 nM (ranged from 0.1 to 73.2 nM) and lowest mean seawater pCO_2 level of 337 ± 50 μatm (ranged from 221 to 411 μatm) over the entire cruise. Significant variations of surface seawater DMS and pCO_2 in the seasonal ice zone (SIZ) of SO were observed, which are mainly controlled by biological process and sea ice activity. We found a significant negative relationship between DMS and pCO_2 in the SO SIZ using 0.1° resolution, $[DMS]_{seawater} = -0.160 [pCO_2]_{seawater} + 61.3$ ($r^2 = 0.594$, $n = 924$, $p < 0.001$). We anticipate that the relationship may possibly be utilized to reconstruct the surface seawater DMS climatology in the SO SIZ. Further studies are necessary to improve the universality of this approach.

1. Introduction

The Southern Ocean (SO) exerts a strong influence on global biogeochemical cycles and air-sea gas fluxes [*Tortell and Long*, 2009]. It has been identified as a strong sink for atmospheric CO_2 [*Landschützer et al*., 2015; *Sabine et al*., 2004] and a significant source for the climate-active gas dimethyl sulfide (DMS) in regions south of 50°S [*Curran and Jones*, 2000; *Inomata et al*., 2006; *Kettle et al*., 1999; *Lana et al*., 2011]. Emissions of Anthropogenic CO_2 to the atmosphere are resulting in a relentless and significant rise in global temperature [*Allen et al*., 2009] and an unprecedented increase in ocean acidity [*Caldeira and Wickett*, 2003], while DMS emitted from the ocean is speculated to have a cooling effect due to its impact on particle and cloud condensation nuclei number concentrations [*Charlson et al*., 1987; *Vogt and Liss*, 2009]. Therefore, investigations for temporal and spatial distributions and air-sea exchange of DMS and CO_2 in the SO will be necessary to further understand their influence on climate change.

Compared to other regions, the SO has been undersampled with respect to surface seawater DMS (south of 40°S, NOAA-Pacific Marine Environmental Laboratory (PMEL) DMS database, http://saga.pmel.noaa.gov.dms). Most former studies in the SO relied on discrete sampling and lab measurements, which were time-consuming and insufficient for high-resolution observations [*Berresheim*, 1987; *Curran et al*., 1998; *Inomata et al*., 2006; *Kiene et al*., 2007; *Staubes and Georgii*, 1993]. Recently, the membrane inlet mass spectrometry has been used for high-resolution survey of DMS in the SO [*Tortell and Long*, 2009; *Tortell et al*., 2011, 2012]. They observed significant changes in surface seawater DMS and pCO_2 over time scales of days to weeks and subkilometer spatial scales. However, these observations were generally conducted in polynyas along the coastal regions, such as Ross Sea and Amundsen Sea. Other important regions of the SO, particularly along the marginal ice zone (MIZ), where there is high phytoplankton biomass or primary production

[*Ishii et al*., 2002; *Taylor et al*., 2013; *Park et al*., 1999], are still lacking fine-resolution surface seawater DMS investigation.

Furthermore, it is hard to model surface DMS concentrations in the seasonal sea ice zone (SIZ) of the SO due to the scarcity of field measurements and the influence of sea ice dynamics on DMS concentrations [*Lana et al*., 2011]. On the other hand, remote sensing provides another way to estimate DMS concentrations by linking remotely sensed parameters like chlorophyll *a* (Chl *a*) and mixed layer depth (MLD) to field-measured DMS concentrations [*Simó and Dachs*, 2002]. Recently, *Kameyama et al*. [2013] found evidence for a strong positive relationship between DMS and net community production (NCP) in the North Pacific Ocean. They anticipated that this relationship could be found in other regions with high primary production, such as the SO, and that surface seawater DMS concentrations could be reconstructed by the empirical relationship of DMS and NCP. Thus, it is possible that the DMS could be reconstructed by remotely derived NCP [*Chang et al*., 2014].

Indeed, there are two aspects related to the impact of the carbon system on sulfur biogeochemical cycling:

1. DMS concentrations appear to be sensitive to ocean acidification. Previous studies reported that seawater DMS concentrations were reduced under high seawater pCO_2 conditions [*Park et al*., 2014; *Archer et al*., 2013], and global DMS emissions may decrease as a result of bombined effects of ocean acidification and climate change [*Six et al*., 2013].
2. The relationship between primary production and sulfur compounds in natural seawater. *Tortell and Long* [2009] and *Tortell et al*. [2011, 2012] investigated the relationships between DMS, pCO_2, andΔO_2/Ar (an index of NCP) in the SO polynyas. Their results indicated that DMS was strongly correlated with pCO_2 and ΔO_2/Ar during spring in the Ross Sea but decoupled from pCO_2 and ΔO_2/Ar during summer in the Ross Sea and Amundsen Sea. As phytoplankton activity can strongly impact both the carbon cycle and sulfur cycle, linkages between the parameters of the carbon cycle and sulfur cycle seem reasonable.

At present, numerous SO surface pCO_2 data are available through the SOCAT database (http://www.socat.info/). If sufficient numbers of field DMS measurements are available and the significant linkage between DMS and pCO_2 is demonstrated, it is possible to develop an algorithm to reconstruct the surface DMS distribution using the pCO_2 data from the SOCAT database. In this study, we performed high-resolution surface seawater DMS and pCO_2 measurements from the SO during the 30th Chinese Antarctic Research Expedition (CHINARE-Ant30th). The factors driving the surface DMS and pCO_2 distributions were analyzed in the distinct oceanic regions. The relationship between DMS and pCO_2 was also detailed and examined. We propose that the relationship could be possibly used in the reconstruction of surface seawater DMS in SO SIZ.

2. Materials and Methods

2.1. Study Area

The SO is a typical high-nutrient and low-chlorophyll area due to iron (Fe) limitation [*Boyd et al*., 2000], in which primary production in the pelagic ocean is generally low with little variation [*Arrigo et al*., 1998]. However, in the SO SIZ, primary production exhibits great variability and it is strongly impacted by sea ice retreat and melting [*Taylor et al*., 2013; *Smith and Comiso*, 2008; *Wang et al*., 2014]. Particularly in the MIZ, phytoplankton blooms are common. The MIZ has been associated with the retreating sea ice edge and is defined operationally as the area where sea ice is present at the beginning of the retreat but not at the end [*Arrigo et al*., 1998]. The variance of phytoplankton activity and sea ice conditions in the SO could certainly impact the biogeochemical cycle of gases, such as DMS and CO_2 [*Tortell and Long*, 2009].

Our measurements were conducted on board the *R/V Xue Long* in February–April 2014 during CHINARE-Ant30th. The ship tracks were from Drake Passage, SO to the East China Sea (Leg 1, named as west-east transect: from Drake Passage to Prydz Bay, 7–24 February 2014; Leg 2, named as south-north transect: from Prydz Bay to Fremantle, Australia, 26 February to 16 March 2014, and from Fremantle, Australia, to East China Sea, 22 March to 11 April 2014). The entire cruise track was about 28,000 km and the main part of transect traversed the Atlantic Ocean Sector and Indian Ocean Sector of the SO. In general, most of the west-east transect was located in the MIZ (Figure 1).

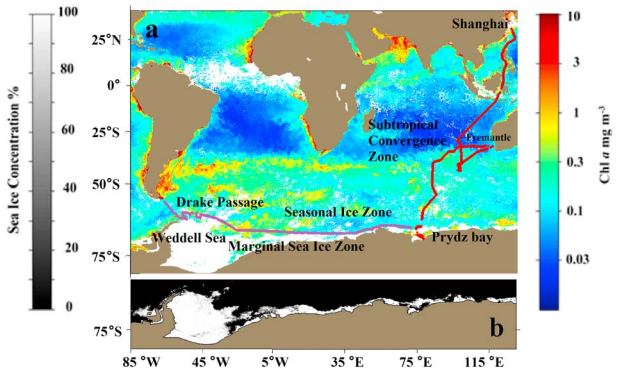

Figure 1. (a) The transect during the thirtieth Chinese National Antarctica Research Expedition (purple line is the west-east transect; red line is the south-north transect). The background is the monthly averaged Chl *a* concentration (color scale), and the white color represents areas where Chl *a* is undetectable; (b) daily sea ice distribution along the transect from 9 to 28 February 2014 (gray scale).

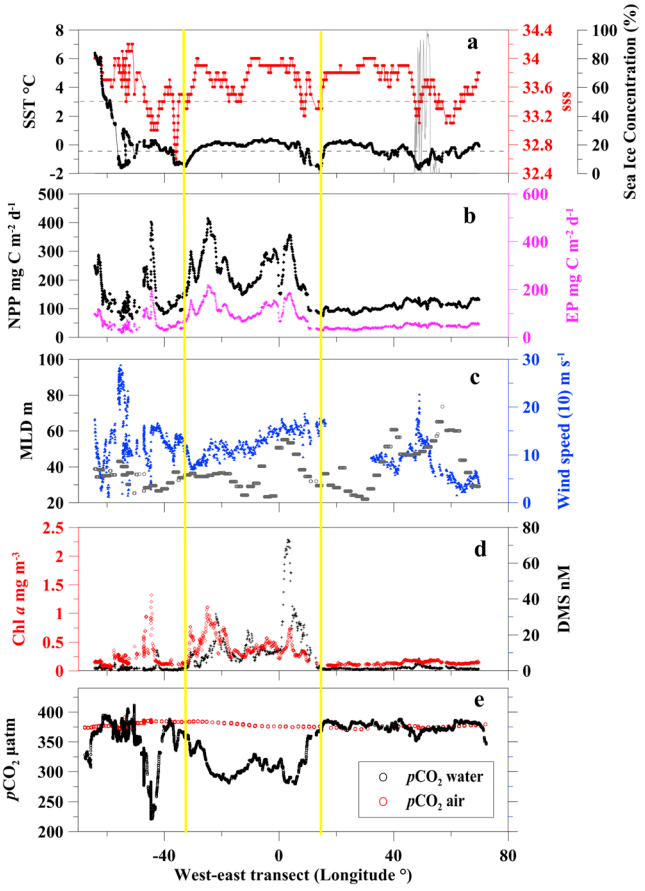

Figure 2. The distribution of (a) surface seawater temperature (SST), salinity (SSS), sea ice concentration (grey); (b) monthly averaged NPP and EP; (c) MLD (grey) and wind speed; (d) DMS and monthly average Chl *a* (red); (e) surface seawater pCO_2, and atmospheric pCO_2 in the west-east transect. Note that the data between the yellow lines are the high DMS levels located in the MIZ.

2.2. Chemical Analyses

A custom-built automatic purge and trap system coupled with gas chromatography-pulsed flame photometric detection (Trace GC, Thermo Company, USA) was utilized for shipboard underway continuous measuring of surface seawater DMS. Details of the method and calibration procedure are described by *Zhang and Chen* [2015]. The surface seawater samples were continuously introduced to the analysis system through the ship's seawater pump system at 4 m depth. The sample rate of this system is 10 min^{-1} and the detection limit is 0.05 nM. The ship cruising speed was about 10–15 knots in sea ice areas, which led to a spatial sample resolution of 3–4.5 km.

An automatic system (GO Flow pCO_2 system, Model 8050, General Oceanic Inc., Miami FL, USA) was installed on board for underway pCO_2 observations, and calibration was done using CO_2 standard gases from National Oceanic and Atmospheric Administration (NOAA) with concentrations of 244.25, 366.86, and 546.98 ppmv (CO_2/air). The measurement method was the same as described in *Gao et al.* [2012]. The sampling interval was about 3 min and the system was calibrated every 2.5 h. The accuracy was estimated to be better than 2 μatm for seawater pCO_2.

Sea surface temperature (SST) and salinity (SSS) were determined continuously by the shipboard underway conductivity-temperature-depth system (SBE21, USA) at a sampling interval of 5 s. In addition, meteorology data, such as wind speed and air pressure, were obtained from the shipboard meteorology observation system run by National Marine Environmental Forecasting Center of China. The GPS information was

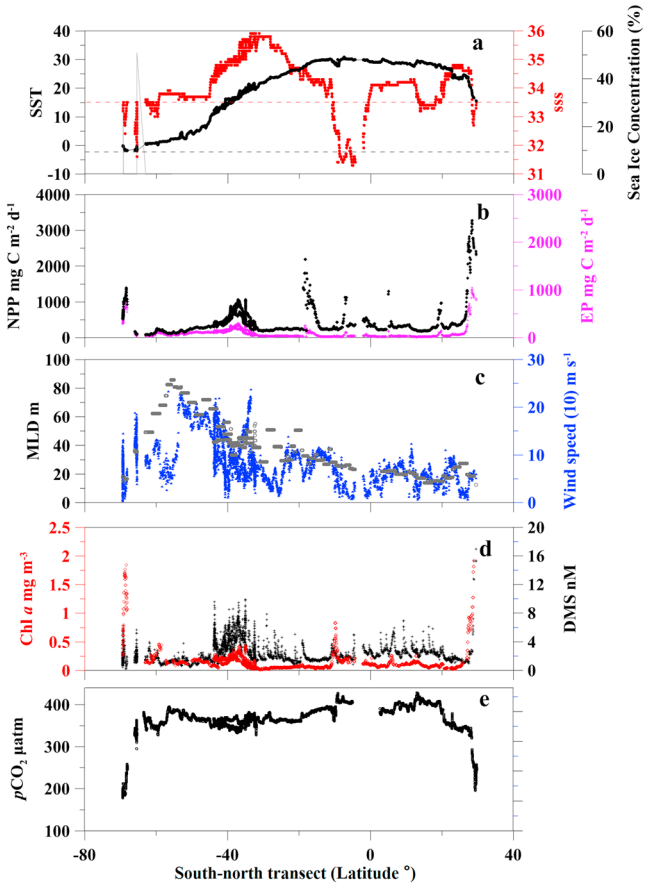

Figure 3. The distribution of (a) surface seawater temperature (SST), salinity (SSS), sea ice concentration (grey); (b) monthly average NPP and EP; (c) MLD (grey) and wind speed; (d) DMS and 8 day average Chl *a* (red); (e) surface seawater pCO_2 (the atmospheric pCO_2 was not measured) in the south-north transect.

obtained from the shipboard GPS record, providing the sampling positions of DMS and pCO_2.

2.3. Acquisition of Remote Sensing Data

The 8 day and monthly average remotely sensed Chl *a* data were downloaded from the Aqua Moderate Resolution Imaging Spectroradiometer (MODIS) website (http://oceancolor.gsfc.nasa.gov/) with a spatial resolution of 9 km. We did not use the daily data due to inconsistent data coverage over most of the ship track. We matched the 8 day and monthly average data with the DMS data obtained in the field using latitude, longitude, and time of measurement, and made the comparison of the matching ratio (number of Chl *a* data matched/number of DMS data). When using 8 day average Chl *a* data, the matching ratios were 44.98% and 80.01% in west-east transect and south-north transect, respectively. More favorable matching ratios, 82.39% and 90.16%, were achieved in west-east transect and south-north transect when using monthly average data. Please also see the comparison between 8 day and monthly average Chl *a* data along the transects in the supporting information (Figure S1). We found that there is general agreement between them. Thus, we decided to use the monthly average Chl *a* in west-east transect and 8 day average Chl *a* data in south-north transect for our discussion.

The daily sea ice concentrations along the transects were obtain from the University of Bremen (http://www.iup.uni-bremen.de:8084/amsr2/ and Figure 1), with a spatial resolution of 6.25 km [*Spreen et al.*, 2008]. The sea ice concentration distributions were presented in Figures 2a and 3a along the transect. Most of the ship track in the SO is not far from the sea ice margin. There were only a few areas of the ship track with high sea ice concentrations due to the fact that the icebreaker usually avoided high sea ice concentration areas for safety concern. In addition, when the ship was in heavy sea ice conditions, the DMS and pCO_2 observations were stopped to avoid potential damage to the water pump.

Mixed layer depth (MLD) has been shown to be an important parameter in reconstructing DMS concentrations at the surface ocean [*Simó and Dachs*, 2002]. Here we use the global monthly MLD climatology data from Institut Français de Recherche pour l'Exploitation de la Mer (http://www.ifremer.fr/cerweb/deboyer/mld/Surface_Mixed_Layer_Depth.php) with a resolution of 2° × 2° grid, which was estimated from a fixed threshold on density profiles [*Clément et al.*, 2004].

$$\text{MLD} = \text{depth where } \left(\sigma_0 = \sigma_{010\text{m}} + 0.03 \text{ kg m}^{-3}\right) \quad (1)$$

The criterion selected is a threshold value of density from a near-surface value at 10 m depth ($\Delta\sigma_\theta$ = 0.03 kg m^{-3}). The MLD data in the south-north transect are correlated with the variation of field wind speed data (Figure 3), but the two values are not always correlated in the west-east transect (Figure 2). This may be explained by the fact that the MLD data are from monthly climatology, which may not represent the field condition along the ship track.

Net primary production (NPP) is defined as the remaining photosynthetic products that are available for phytoplankton growth or consumption by the heterotrophic community. In the Vertically Generalized Production Model [*Behrenfeld and Falkowski*, 1997], oceanic NPP is a function of Chl *a*, available light, and the photosynthetic efficiency. Monthly NPP data were obtained from the Ocean Productivity website (https://orca.science.oregonstate.edu), where the standard product is based on MODIS Chl *a*, MODIS sea surface temperature, Sea-viewing Wide Field-of-view Sensor PAR (photosynthetically available radiation), and estimates of euphotic zone depth from a model developed by *Morel and Berthon* [1989]. The export production (EP), the portion of primary production driven by externally supplied nutrients ("new" production) when a steady state nutrient budget with a constant elemental organic matter stoichiometry is assumed for the euphotic zone [*Dunne et al*., 2005], was estimated as the following equation by *Laws et al*. [2011]:

$$Ef = ((0.5857 - 0.0165\,T)\times p)/(51.7 + p) \quad (2)$$

Ef is the EP to NPP ratio, *T* is SST (°C), and *p* is the NPP in mg C m^{-2} d^{-1}. Equation (2) accounts for 87% of the variance in the observed *Ef* ratios in global ocean [*Laws et al*., 2011]. The estimated EP and NPP data can be utilized to explain the surface seawater DMS and pCO_2 variance.

3. Results and Discussion

3.1. Sea Ice Distribution and Surface Water Hydrography

Our study area consisted of two distinct transects: one was mainly located in the SO MIZ (west-east transect) and the other one traversed from the SO to the East China Sea (south-north transect). During the time of survey in the west-east transect, the sea ice melting rate was slow and the sea ice extent was close to the minimum level of the year. In the area south of 60°S (transect from 60°W to 75°E), SST and SSS varied from −1.7°C to 1.0°C and from 34.2 to 32.8, respectively. In the SO, the temperature and salinity of surface water masses were significantly influenced by surface warming and sea ice melting. The waters with SST < -0.5°C (black dash line in Figure 2a) and SSS < 33.4 (red dash line in Figure 2a) were identified as a residual ice melt signals in these regions [*Tortell et al*., 2012]. The influence of sea ice melting on the surface waters was found along the west-east transect, where there were cold water areas (SST < -0.5°C) associated with relatively low salinity (SSS < 33.4). Around 50°E, we observed high sea ice concentrations corresponding with low-temperature and low-salinity seawater. In addition, we could not find waters significantly impacted by circumpolar deep water (CDW, warm water with high salinity, $T > 1$°C, $S > 34.7$) along the transect.

In the south-north transect, a strong latitudinal gradient of SST (range from −1.8°C to 30.9°C) and SSS (range from 31.3 to 35.9) was clearly visible (Figure 3). In general, SSS was more variable than SST along this transect. A maximum SSS of 35.9 was found around 32°S and decreased both southward and northward. The fluctuations in SSS in the Prydz Bay (~2) could be attributed to the formation of sea ice at the end of February, which could increase the salinity of seawater. Along the transect from 58°S to 42°S, SSS exhibited a small variance, while there was significant increase of SST from south to the north. These features are due to the eastward flow of the Antarctic Circumpolar Current (ACC), which is driven by the world's strongest westerly winds (wind speed >10 m s^{-1}). North of the ACC, from 32°S to 42°S, we observed a large change of SST (>5°C) and SSS (>0.5), which was identified as the Subtropical Front (STF) [*Orsi et al*., 1995] and Subtropical Convergence Zone (SCZ). In contrast, a noticeable decline of SSS at the equator was observed, likely due to the input of freshwater from continental runoff and rainfall. In the East China Sea, the observed decline of SSS and SST is the result of freshwater input from the Yangtze River.

3.2. The Distributions of Satellite Derived Chl *a*, NPP, and EP

Distributions of Chl *a*, NPP, and EP along the transects are presented in Figures 2b, 2d, 3b, and 3d. Monthly average Chl *a* in the west-east transect and 8 day average Chl *a* in south-north transect were

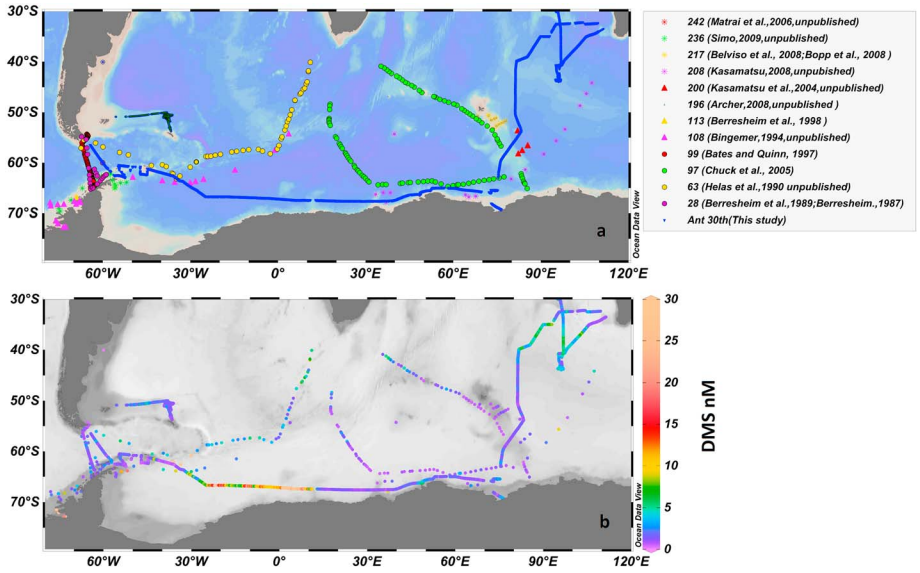

Figure 4. Comparison of the surface seawater DMS data in this study with data from previous studies. (a) Sampling location. (b) DMS concentrations (shown with the color bar and note that the scale is capped at 30 nM to ensure readability of the plots). The previously acquired data were downloaded from NOAA-PMEL DMS database for the months of February and March. The chosen area was mostly located in the Indian Ocean sector and Atlantic Ocean sector of the SO.

0.25 ± 0.19 mg m^{-3} (0.06–1.32 mg m^{-3}) and 0.18 ± 0.21 mg m^{-3} (0.01–1.92 mg m^{-3}), respectively, with variability similar to NPP and EP. The mean NPP and EP values were 155 ± 74 mg C m^{-2} d^{-1} (range: 62–415 mg C m^{-2} d^{-1}), 69 ± 41 mg C m^{-2} d^{-1} (range: 20–218 mg C m^{-2} d^{-1}), and 439 ± 335 mg C m^{-2} d^{-1} (range: 78–3277 mg C m^{-2} d^{-1}), 116 ± 122 mg C m^{-2} d^{-1} (range: 12–1048 mg C m^{-2} d^{-1}) in west-east and south-north transects, respectively.

In the west-east transect, significant variance of Chl *a*, NPP, and EP was found and the high values were mostly located in the MIZ of Weddell Sea (40°W–50°W) and Indian Ocean Sector (35°W–15°E). The estimated NPP and EP in the MIZ are lower than the modeled monthly average primary production (PP) in the SO water from the study by *Arrigo et al*. [1998], in which relatively high PP values (750 mg C m^{-2} d^{-1} and 610 mg C m^{-2} d^{-1}) were estimated in the MIZ of Weddell Sea and Indian Ocean Sector of SO in February. In addition, *Smith and Nelson* [1990] reported that seasonal (from November to March) average new production in the MIZ of Weddell was at least 325 mg C m^{-2} d^{-1}.

In the south-north transect, the relatively high Chl *a*, NPP, and EP were found in the polynya of Prydz Bay, the MIZ around 60°S, the SCZ, and the East China Sea. NPP and EP values ranged from 523 to 1397 mg C m^{-2} d^{-1} and from 284 to 827 mg C m^{-2} d^{-1}, respectively, in the polynya of Prydz Bay. Such high variability is likely due to the onset of sea ice formation around the polynya at the beginning of March, which has been shown to enhance phytoplankton biomass [*Lizotte*, 2001; *Zhang et al*., 2015]. The relatively high phytoplankton activity from 32°S to 42°S was located in the STF and SCZ, where the strong stratification and ample solar radiation caused the growth of phytoplankton [*Llido et al*., 2005]. The highest NPP and EP, with high Chl *a*, were found in the East China Sea, where sufficient light and nutrients were the main factors that impacted phytoplankton activity.

3.3. Spatial Distributions of Surface Seawater DMS

3.3.1. West-East Transect

In the west-east transect, DMS concentrations exhibited large spatial variations with a mean value of 5.0 ± 9.7 nM, ranging from 0.1 to 73.2 nM (Figure 2a). The observations along the SIZ demonstrated that the distributions of DMS were not homogeneous. It is noteworthy that the observations from our cruise track filled the gaps of previous observations in the same region during the same time period (Figure 4).

As shown in Figure 4, our DMS data obtained along the transects were consistent with the previous observations collected in the NOAA-PMEL DMS database. Clearly, large-scale high-DMS levels located in MIZ from 34°

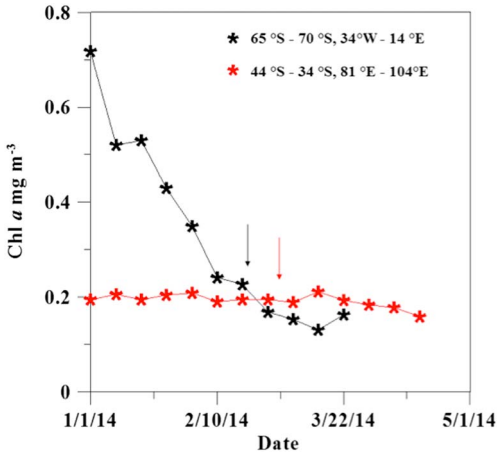

Figure 5. The variations of 8 day average Chl *a* values in chosen regions from January to May 2014. High levels of seawater DMS were found in these two regions. The arrows indicate the sampling time of DMS during this period. Note that the average Chl *a* values are calculated from averaging the satellite grid Chl *a* data in Chosen regions.

W to 14°E was observed (Figure 4). The position of this high DMS area was slightly east of that in the *Lana et al.* [2011] climatology for February. Our results were in agreement with many previous studies, in which high DMS levels commonly occur in the surface water of the MIZ [*Curran et al.*, 1998; *Inomata et al.*, 2006; *Kettle et al.*, 1999], related to the high phytoplankton biomass there. The maximum DMS concentration during the cruise, 73.2 nM, was found around 3°E. This value is several times higher than previously reported values (27 nM [*Turner et al.*, 1995], 22 nM [*Curran et al.*, 1998], and 15.8 nM [*Inomata et al.*, 2006]). However, it is lower than the observation of 88 nM in the MIZ of Weddell Sea by *Fogelqvist* [1991]. The average Chl *a* value in this large-scale high-DMS region (from 34°W to 14°E) drastically declined in the January, suggesting that high levels of DMS occurred after the bloom (Figure 5, black line). Microzooplankton grazing and massive death of algae can enhance the DMS concentration [*Stefels et al.*, 2007]. In the later summer of the SO SIZ, diatoms (with low intracellular DMSP content) are likely the main phytoplankton species [*Boyd*, 2002]. These factors may explain the decoupling between the DMS and Chl *a* here.

Additionally, we found a DMS concentration peak (as high as 6.8 nM) around 50°E, corresponding with high sea ice concentrations. Previous studies have demonstrated that significant DMS and DMSP (dimethylsulphoniopropionate, the precursor of DMS) levels (>100 nM) were observed under the sea ice bottom, coincident with very high Chl *a* values [*Trevena and Jones*, 2012, 2006]. Addtionally, during the melting seasons, the DMS or DMSP from the sea ice bottom could be released into the surrounding waters. As described in section 3.1, we observed the influence of sea ice melt around 50°E; therefore, the high DMS levels there are likey be due to high DMS and DMSP concentrations in the sea ice.

3.3.2. South-North Transect

In the south-north transect, a distinct DMS distribution pattern in the different regions of the cruise track was observed (Figure 3d). Over the entire south-north transect DMS levels ranged from 0.2 nM to 16.9 nM with an average value 2.6 ± 1.6 nM.

High DMS concentrations (up to 9.8 nM), corresponding to high levels of Chl *a*, were found near 40°S in the STF, where SSS was also high. The high DMS concentrations in the STF are similar to previous observations (Figure 4). High SSS in this region can increase intracellular DMSP production, possibly leading to high DMS levels [*Stefels et al.*, 2007]. Moreover, the high irradiance there promotes shallower MLDs (~40 m), with consequences both for DMS release from stressed algal cells and inhibition of bacterial DMS consumption [*Lizotte et al.*, 2012; *Simó and Pedros-Alio*, 1999; *Vallina and Simó*, 2007; *Vila-Costa et al.*, 2014]. As shown in Figure 5 (red line), the average Chl *a* in this high DMS area was invariable from January to May, suggesting that the DMS concentrations may be stable in this region.

The average DMS concentration between 15°S and 15°N was 2.4 ± 0.8 nM (range: 0.8 nM to 6.9 nM, n = 761). The mean value is higher than that observed at the equatorial region of the west Pacific Ocean (mean value: 0.9 nM) [*Zindler et al.*, 2013; *Marandino et al.*, 2013], but it is in agreement with the measurements by *Bates and Quinn* [1997], who reported that the surface seawater DMS mean level is relatively constant both seasonally and interannually (2.7 ± 0.7 nM) in the middle equatorial Pacific Ocean (15°S ~ 15°N) from 1982 to 1996.

DMS concentrations rapidly increased upon entry into the East China Sea, up to values of 16.9 nM (Figure 3d), coincident with variations in the Chl *a* concentrations. High DMS levels in the surface water of the East China

Table 1. The Mean Levels of DMS and pCO_2 and Correlations Between DMS, pCO_2, Chl *a*, NPP, EP, SST, SSS, Air Pressure (P) and Wind Speed (*U*, m s^{-1}) in the Different Regions Outlined in the Text (Pearson Correlations)[a]

Zones		Mean Value	Chl *a*	NPP	EP	SST	SSS	*U*	DMS Versus pCO_2
≤58°SSIZ	DMS	4.1 ± 8.3	0.395**	0.309**	0.309*	0.047	0.212**	0.303**	−0.495**
		n = 2166	*n* = 978	*n* = 1160	*n* = 1159	*n* = 1164	*n* = 1164	*n* = 1012	*n* = 987
	pCO_2	337 ± 50	−0.682**	−0.706**	−0.730**	−0.002	0.043	−0.346**	
		n = 8592	*n* = 780	*n* = 945	*n* = 929	*n* = 930	*n* = 930	*n* = 804	
58°S–42°SSAAZ	DMS	2.4 ± 1.5	−0.067	0.543**	0.427	0.607**	0.575**	−0.010	−0.245**
		n = 726	*n* = 161	*n* = 161	*n* = 161	*n* = 161	*n* = 161	*n* = 159	*n* = 143
	pCO_2	362 ± 13	−0.225**	−0.749**	−0.755**	−0.706**	−0.457	−0.158	
		n = 2602	*n* = 143	*n* = 143	*n* = 143	*n* = 143	*n* = 143	*n* = 142	
42°S–15°SSSCZ	DMS	3.1 ± 1.8	0.765**	0.246**	0.689**	−0.650**	0.048	−0.066	−0.494**
		n = 1882	*n* = 264	*n* = 268	*n* = 268	*n* = 268	*n* = 268	*n* = 268	*n* = 263
	pCO_2	360 ± 10	−0.607**	0.198**	−0.367**	0.694**	−0.266**	−0.116	
		n = 5868	*n* = 259	*n* = 263	*n* = 263	*n* = 263	*n* = 263	*n* = 263	
15°S–15°NEZ	DMS	2.4 ± 0.8	0.052	−0.078	−0.063	−0.376**	0.212	−0.067	−0.245**
		n = 761	*n* = 249	*n* = 270	*n* = 270	*n* = 274	*n* = 274	*n* = 267	*n* = 205
	pCO_2	396 ± 12	−0.003	−0.005	−0.009	−0.078	−0.463**	−0.393**	
		n = 1976	*n* = 185	*n* = 201	*n* = 201	*n* = 205	*n* = 205	*n* = 198	
15°N–30°NNSCZ	DMS	2.2 ± 1.8	0.555**	0.374**	0.465*	−0.378**	−0.495**	0.165**	−0.406**
		n = 395	*n* = 120	*n* = 140	*n* = 140	*n* = 140	*n* = 140	*n* = 140	*n* = 131
	pCO_2	356 ± 42	−0.691**	−0.662**	−0.725*	0.934**	−0.317**	−0.033	
		n = 1359	*n* = 114	*n* = 131	*n* = 131	*n* = 131	*n* = 131	*n* = 131	

[a]The number of samples is shown below the corresponding correlation.
*The correlation is significant at the 0.05 level (two tailed).
**The correlation is significant at the 0.01 level (two tailed).

Sea have also been observed in previous studies [*Yang et al*., 2012, 2011]. Additionally, the increase of DMS concentrations was also associated with a strong decrease of SSS and SST, indicating that the water input from Yangtze River may impact DMS concentrations [*Yang et al*., 2012].

3.4. Spatial Distributions of Surface Seawater pCO_2

Surface seawater and air pCO_2 levels were measured during the cruise (Figures 2e and 3e). The mean values of seawater pCO_2 were 347 ± 40 μatm (221–411 μatm) and 357 ± 39 μatm (178–428 μatm) in the west-east and south-north transects, respectively. The average pCO_2^{air} was 378 ± 4 μatm in west-east transect, but pCO_2^{air} data were missing for the south-north transect. According to the computed values of ΔpCO_2 ($pCO_2^{seawater} - pCO_2^{air}$), a critical parameter in the CO_2 air-sea flux calculation [*Wanninkhof*, 1992], the SO and East China Sea are a strong sink for atmospheric CO_2, while other regions of cruise track were identified as weak sinks or sources of atmospheric CO_2 (Table 1). Overall, the variation of pCO_2 during the cruise generally correlated with Chl *a*, NPP, and EP.

Significant variations of surface seawater pCO_2 were found in the west-east transect (Figure 2e). These results are consistent with our previous campaign conducted in the SO [*Chen et al*., 2004], during which the distribution of pCO_2 exhibited the same spatial distribution pattern. The strong atmospheric CO_2 sink was found in the Atlantic Sector of the SO (34°W–14°E) due to the large ΔpCO_2 and relatively high wind speed (Figures 4d and 4e). *Stoll et al*. [2002] also reported large-scale surface seawater CO_2 undersaturation in the 65°S–70°S MIZ of the Atlantic Sector of the SO in austral summer, coinciding with high Chl *a* content. Additionally, in the area west of 40°W, strikingly low seawater pCO_2 levels (down to 221 μatm) were observed. The largest ΔpCO_2 in the west-east transect was simultaneously observed (157 μatm). These low seawater pCO_2 levels may not only be impacted by biological activity but also melting sea ice (as SSS values <33.4 were observed). It has been reported that sea ice and its meltwater contain very low levels of pCO_2 [*Cai et al*., 2010]. The values measured around 50°E (~360 μatm) also appear to be impacted by meltwater, since the sea ice concentration was high and relatively low phytoplankton biomass was detected.

In the south-north transect, surface seawater pCO_2 levels presented relatively smaller variations than the west-east transect, except for the measurements in the Prydz Bay and East China Sea (Figure 3e). In the Prydz Bay, we found very low seawater pCO_2 levels, with a mean value of 198 ± 17 μatm (*n* = 523), ranging from 178 μatm to 258 μatm. The seawater pCO_2 increased with latitude until the heavy ice region was

crossed. The enhancement of pCO_2 there was in agreement with our previous study, and the upwelling of CDW around 64°S is likely the main reason [*Gao et al*., 2008]. Around 60°S, we observed a slight decrease of seawater pCO_2 (328 μatm), which was associated with a Chl *a* peak. Between 42°S and 58°S, where wind speed was very high (>10 m s^{-1}, Figure 3c), the seawater pCO_2 average value was 362 ± 13 μatm, indicating a weak sink for atmospheric CO_2 (Table 1). The values are similar to those measured in previous studies [*Metzl et al*., 1999, 1991; *Poisson et al*., 1993]. In the region around 40°S (STF), a large-scale feature of slightly low seawater pCO_2 levels (average value: 346 ± 4 μatm, $n = 679$, range: 335 μatm to 365 μatm) was found, which was not only coincident with the relatively high Chl *a* but also with relatively high SST. North of the SCZ, seawater pCO_2 gradually increased and it exceeded the atmospheric pCO_2 level (approximately 380 μatm) in the equatorial region. The average seawater pCO_2 in the equatorial region between 15°S and 15°N was 397 ± 11 μatm, ranging from 361 μatm to 428 μatm ($n = 2369$), suggesting that the equatorial region is a significant source of CO_2 to the atmosphere. The seawater pCO_2 levels started decreasing again around 20°N, and the lowest seawater pCO_2 levels on this transect were found in the East China Sea (196 μatm).

3.5. Correlations Between DMS, pCO_2, and the Environmental Parameters

The values of DMS, pCO_2, Chl *a*, NPP, EP, SST, SSS, and wind speed were binned by 0.1° along longitude (west-east transect) or latitude (south-north transect) and correlated with each other (Table 1). Chl *a*, NPP, and EP data were obtained using a remote sensing method, and the other parameters were measured directly on board. We separated the data into five zones: (1) The region south of 58°S (≤58°S), most of which is located in the SO SIZ (named as SIZ); (2) The region between 58°S and 42°S, located in the sub-Antarctic zone and Antarctic zone (named as SAAZ) [*Curran et al*., 1998]; (3) The region between 42°S and 15°S located in the south SCZ (named as SSCZ); (4) The region between 15°S and 15°N, located in the equatorial zone as indicated by *Bates and Quinn* [1997] (named as EZ); and (5) The region between 15°N and 30°N, located in the north SCZ (named as NSCZ).

We found that DMS and Chl *a* are significantly positively correlated in the SSCZ region ($r = 0.765$, $p < 0.01$), moderately positively correlated in the NSCZ ($r = 0.555$, $p < 0.01$), and weakly positively correlated in the SIZ ($r = 0.395$, $p < 0.01$) but not correlated in the SAAZ and EZ regions. These results are consistent with the majority of publications indicating that the relationship between seawater DMS and Chl *a* is not always straightforward in the oceans. Therefore, the relationship between Chl *a* and DMS cannot be used to predict DMS distributions in the global ocean. We found that DMS is significantly correlated with EP ($r = 0.689$, $p < 0.01$) in the SSCZ region, but in the other regions, only weak positive correlations or no relationships were found. In the case of relationships between DMS and NPP, no correlations or weak positive correlations were computed in all regions. Although the high DMS levels are consistent with the high values of NPP and EP in the high production regions, the overall low linear correlations seem to disagree with the findings of *Kameyama et al*. [2013]. Additionally, our result in the SO is consistent with the findings during the SO summer, in which the DMS concentrations were not correlated with $\Delta O_2/Ar$ (an index of NCP) [*Tortell et al*., 2011].

In the SIZ and SAAZ regions, the surface seawater pCO_2 values are significantly negatively correlated with NPP and EP ($r > 0.7$, $p < 0.01$). However, pCO_2 levels are strongly associated with Chl *a* ($r = -0.682$, $p < 0.01$) in the SIZ but weakly negatively correlated with Chl *a* in the SAAZ region ($r = -0.225$, $p < 0.01$). The results demonstrate that surface seawater pCO_2 was strongly impacted by biological activity in the SO [*Takahashi et al*., 2002]. In contrast, we found that seawater pCO_2 was not only significantly correlated with phytoplankton biomass but also strongly associated with SST in both the SSCZ and NSCZ regions, indicating that SST was also an important factor. The rising temperature can cause the decrease of the CO_2 solubility, thereby increasing the pCO_2 levels [*Takahashi et al*., 1993]. However, in the equatorial region, we could not find correlations between seawater pCO_2 and any other parameters.

3.6. Relationships Between DMS and pCO_2

Comparison of the concentration variations for DMS and pCO_2 shows that they tended to vary inversely (Figures 2 and 3). *Tortell and Long* [2009] and *Tortell et al*. [2011, 2012] observed a large range of correlations between DMS and pCO_2 in the SO (r value ranged from −0.03 to −0.73). In this study, we also investigated the relationship between the DMS and pCO_2 in different oceanic regions. As shown in Table 1, moderate negative correlations between DMS and pCO_2 are found in the SIZ ($r = -0.495$, $n = 987$, $p < 0.01$), SSCZ ($r = -0.494$, $n = 263$, $p < 0.01$), and NSCZ ($r = -0.406$, $n = 131$, $p < 0.01$), while low negative correlations are found in

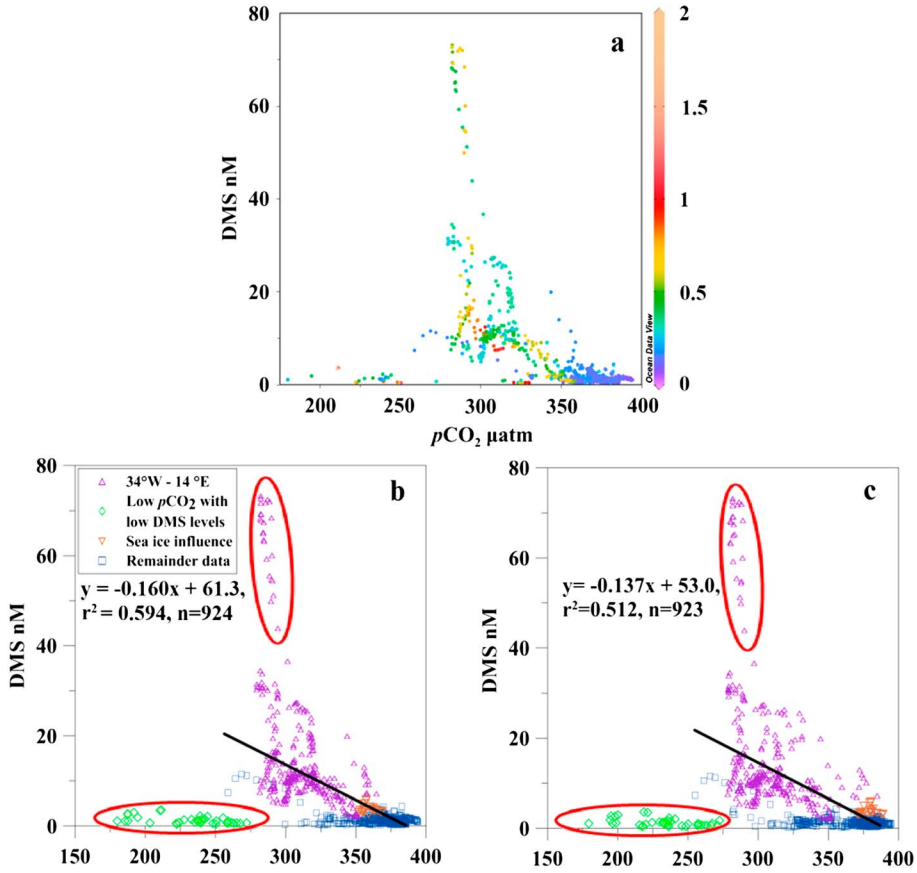

Figure 6. (a) DMS, pCO_2, and Chl *a* in the SIZ. The color bar indicates Chl *a* concentrations in mg m^{-3}. Relationships between DMS and (b) pCO_2 binned to 0.1°; (c) temperature normalized (n-pCO_2) binned to 0.1°. Note that the data in the red circles are the outlier data.

the SAAZ and EZ. The results show that the DMS and pCO_2 correlations are different between the oceanic regions, with the high productivity regions having higher correlation values, such as in the SO SIZ and SSCZ. The correlation between DMS and pCO_2 is better than the correlations between DMS and the other parameters in SO SIZ. This indicates that pCO_2 is a better predictor of DMS concentrations than Chl *a* there (Table 1, see the supporting information Figure S2). Therefore, we provide a more detailed investigation of the DMS and pCO_2 relationship in the SO SIZ.

In the case of the SIZ (Figure 6), the data were divided into four clusters according to the biogeochemical characteristics: (1) high DMS levels and moderate pCO_2 levels with high Chl *a* (purple triangles) located in the region from 34°W–14°E, (2) low DMS and low pCO_2 levels with relatively high Chl *a* (green diamonds) located in Prydz Bay and 43°W–45°W, (3) sea ice influence with low Chl *a* (brown inverted triangles) located near 50°E, and (4) the remainder of the data (blue squares) with low DMS, high pCO_2, and relatively low Chl *a*. These clusters represent most of the DMS and pCO_2 relationships in the SO SIZ. We found that there are two outlier data sets that deviate from the bulk of the data (Figure 6b, the data in red circles). One is characterized by DMS values above 40 nM, and the other one is characterized by pCO_2 levels below 280 µatm. The high DMS values with moderate pCO_2 (DMS $>$ 40 nM) are likely located in the bloom-declining region (from 2°E to 4°E). Larger-scale algae death and possibly zooplankton grazing, in addition to microbiological processes, could rapidly enhance the seawater DMS concentrations. However, the pCO_2 levels have little variance here, likely due to the fact that there is no longer active photosynthesis. The other cluster contains very low pCO_2 levels with low DMS concentrations (green diamond) mainly locating in 43°W–45°W and Prydz Bay. The production of DMS is likely limited at that time due to the dominance of low DMSP-containing algae and/or low

microbial activity. In addition, low pCO_2 levels may be caused by both the uptake by phytoplankton, as well as the sea ice meltwater contribution (e.g., in the region 43°W–45°W).

After excluding the data in the red circles, a significant negative correlation between DMS and pCO_2 was observed ($r^2 = 0.594$, $n = 924$, $p < 0.01$) in the SIZ,

$$[\mathrm{DMS}]_{\mathrm{seawater}} = -0.160\,[pCO_2]_{\mathrm{seawater}} + 61.3 \quad (3)$$

The relationship between DMS and pCO_2 indicates that they have similar controlling factors in the ocean surface, namely, biological activity, air-sea exchange, and sea ice influence. These factors inversely affect the surface ocean DMS and pCO_2 values. For example, high phytoplankton biomass can strongly uptake the CO_2 in seawater while simultaneously producing the precursor of DMS. In addition, air-sea exchange only acts as a sink of the seawater DMS but is a source of seawater CO_2 when the pCO_2 levels in seawater are below the atmospheric CO_2 levels. Finally, as stated above, sea ice melt may enhance DMS concentrations in vicinity waters but dilute the CO_2 contents there.

As described in *Kameyama et al*. [2014], the temperature effect calibration of pCO_2, i.e., n-pCO_2, was used as the index of NCP, and they identified a significant negative correlation ($r^2 = 0.59$, $n = 1263$, $P < 0.001$) between isoprene (a biogenic trace gas) and the n-pCO_2 in the SO. Therefore, the relationship between DMS and temperature-normalized pCO_2 (n-pCO_2) was also investigated, and it was also compared with the nonnormalized values. The temperature effect calibration was done according to the studies by *Kameyama et al*. [2014] and *Takahashi et al*. [1993] as the following:

$$\mathrm{n} - pCO_2 = pCO_2 \times \exp[0.0423(-0.24 - \mathrm{SST})] \quad (4)$$

where −0.24 (°C) was the average temperature value in the region south of 58°S. As shown in Figure 6c, although a moderate negative correlation, $r^2 = 0.512$, is obtained, the r^2 value is lower than the correlation of nonnormalized one, $r^2 = 0.594$. The slope of the temperature-normalized graph (Figure 6c, slope = −0.137) is a little higher than the nonnormalized one (Figure 6b, slope = −0.162). The temperature normalization did not result in a large change in the values of pCO_2 and, consequently, did not reduce the scatter in the pCO_2 data. Therefore, this added step of data normalization did not provide anything useful for the analysis of the relationship between DMS and pCO_2 and we only refer to the nonnormalized pCO_2 data in the rest of the text.

Although previous simulation of surface water DMS presented relative high R^2, e.g., $R^2 = 0.68 \sim 0.84$ by using the MLD and Chl *a* [*Simó and Dachs*, 2002], $R^2 = 0.676$ by using the NCP [*Kameyama et al*., 2013], and $R^2 = 0.63$ by using SST, surface seawater nitrate and latitude [*Watanabe et al*., 2007], they were never tested in polar regions, such as SO SIZ. In addition, the comparison of seven different DMS climatologies, i.e., *Kettle et al*. [1999], *Kettle and Andreae* [2000], *Anderson et al*. [2001], *Aumont et al*. [2002], *Simó and Dachs* [2002], *Chu et al*. [2003], and *Belviso et al*. [2004a], provided that the uncertainty in quantifying the global distritbuion of surface seawater DMS could up to 100% in the high latitudes [*Belviso et al*., 2004b]. In the SO, particularly in the SIZ, the concentrations of DMS are hard to simulate and are possibly underestimated due to the low frequency of sampling [*Levasseur*, 2011]. The satellite products required for the other DMS parameterizations may not be available or reliable in the SO SIZ, while direct measurements of pCO_2 are relatively abundant in the SOCAT database (generally bellow 0.1°). Therefore, we proposed that the strong relationship between DMS and pCO_2 found in SO SIZ could be possibly employed to simulate the surface ocean DMS concentrations there. Although our algorithm can explain 59.4% surface seawater DMS variance in SO SIZ, the algorithm is not applicable in the cases of data in red circles (Figure 6b). Further studies are necessary to improve the universality of this approach.

4. Summary

High-resolution underway measurements of surface seawater DMS and pCO_2 were conducted during the CHINARE Ant30th from February to April 2014. The ship track traversed the Atlantic Ocean Sector and Indian Ocean Sector of the SO, East Indian Ocean, and Northwest Pacific Ocean, and the ship track was approximately 28,000 km. The main purpose of this study was to investigate the spatial distributions and

the controlling factors of surface seawater DMS, and most importantly, its relationship with surface seawater pCO_2 in different regions.

Overall, our study demonstrated that the SO, particularly in the region south of 58°S, had higher mean surface seawater DMS concentrations 4.1 ± 8.3 nM (ranged from 0.1 to 73.2 nM) and lower mean seawater pCO_2 levels 337 ± 50 μatm (ranged from 221 to 411 μatm) compared to those in the east Indian Ocean and northwest Pacific Ocean. Large variations of surface seawater DMS and pCO_2 in the SO SIZ were observed, which might be related to the biological activities. Sea ice dynamics have a large impact on the biological gases, not only through releasing sulfur compounds or diluting CO_2 concentrations but also by impacting phytoplankton activity. Two large-scale high-DMS concentration regions were located in the SO MIZ from 34°W to 14°E and around 40°S in the southeast Indian Ocean.

The driving forces for DMS and pCO_2 were quite different among oceanic regions, which led to different DMS and pCO_2 levels. We found a significant negative relationship between DMS and pCO_2 in the SO SIZ using 0.1° resolution, $[DMS]_{seawater} = -0.160\ [pCO_2]_{seawater} + 61.8$ ($r^2 = 0.594$, $n = 924$, $p < 0.001$). We highlight this equation, as it may have implications for reconstructing DMS values in the SO SIZ. Further studies are necessary to determine the universality of this approach.

Acknowledgments
We thank the Chinese Arctic and Antarctic Administration (CAA) of State Oceanic Administration (SOA) and the crew of R/V *Xue Long* for support with field operations. Furthermore, we would like to extend our thanks to PhD student Yanfang Wu of the University of New South Wales for his assistance with English, discussion and revision of the paper, as well Tobias Steinhoff (GEOMAR, Germany) for his valuable input. This work was supported by the National Natural Science Foundation of China (NSFC) (41476172, 41230529, 41106168, 41406221, and 41476173) and Qingdao National Laboratory for marine science and technology foundation (QNLM2016ORP0109), the Scientific Research Foundation of Third Institute of Oceanography, State Oceanic Administration under contract 2015031, Chinese Projects for Investigations and Assessments of the Arctic and Antarctica (CHINARE2015-16 for 01-04-02, 02-01, 04-04, 04-03 and 03-04-02), and the Chinese International Cooperation Programs (2015DFG22010, IC201201, IC201308, and IC201513), and Korea Polar Research Institute grant PE17060. The study was also supported by the foundation of International Organizations and Conferences and Bilateral Cooperation of Maritime Affairs. Please see the original DMS data in the supporting information or directly contact the author for requesting (zhangmiming@tio.org.cn).

References

Allen, M. R., D. J. Frame, C. Huntingford, C. D. Jones, J. A. Lowe, M. Meinshausen, and N. Meinshausen (2009), Warming caused by cumulative carbon emissions towards the trillionth tonne, *Nature*, *458*(7242), 1163–1166.

Archer, S. D., S. A. Kimmance, J. A. Stephens, F. E. Hopkins, R. G. J. Bellerby, K. G. Schulz, J. Piontek, and A. Engel (2013), Contrasting responses of DMS and DMSP to ocean acidification in Arctic waters, *Biogeosciences*, *10*(3), 1893–1908.

Anderson, T. R., S. A. Spall, A. Yool, P. Cipollini, P. G. Challenor, and M. J. R. Fasham (2001), Global fields of sea surface dimethylsulfide predicted from chlorophyll, nutrients and light, *J. Mar. Syst.*, *30*, 1–20.

Arrigo, K. R., D. Worthen, A. Schnell, and M. P. Lizotte (1998), Primary production in Southern Ocean waters, *J. Geophys. Res.*, *103*, 15,587–15,600, doi:10.1029/98JC00930.

Aumont, O., S. Belviso, and P. Monfray (2002), Dimethylsulfoniopropionate (DMSP) and dimethylsulfide (DMS) sea surface distributions simulated from a global three-dimensional ocean carbon cycle model, *J. Geophys. Res.*, *107*(C4), 3029, doi:10.1029/1999JC000111.

Bates, T. S., and P. K. Quinn (1997), Dimethylsulfide (DMS) in the equatorial Pacific Ocean (1982 to 1996): Evidence of a climate feedback?, *Geophys. Res. Lett.*, *24*, 861–864, doi:10.1029/97GL00784.

Behrenfeld, M. J., and P. G. Falkowski (1997), Photosynthetic rates derived from satellite-based chlorophyll concentration, *Limnol. Oceanogr.*, *42*(1), 1–20.

Belviso, S., L. Bopp, C. Moulin, J. C. Orr, T. R. Anderson, O. Aumont, S. Chu, S. Elliott, M. E. Maltrud, and R. Simó (2004a), Comparison of global climatological maps of sea surface dimethyl sulfide, *Global Biogeochem. Cycles*, *18*, GB3013, doi:10.1029/2003GB002193.

Belviso, S., C. Moulin, L. Bopp, and J. Stefels (2004b), Assessment of a global climatology of oceanic dimethylsulfide (DMS) concentrations based on SeaWiFS imagery (1998–2001), *Can. J. Fish. At. Sci.*, *61*(5), 804–816.

Berresheim, H. (1987), Biogenic sulfur emissions from the Subantarctic and Antarctic Oceans, *J. Geophys. Res.*, *92*, 13,245–13,262, doi:10.1029/JD092iD11p13245.

Boyd, P. W. (2002), Environmental factors controlling phytoplankton processes in the Southern Ocean, *J. Phycol.*, *38*(5), 844–861.

Boyd, P. W., A. J. Watson, C. S. Law, E. R. Abraham, T. Trull, R. Murdoch, D. C. Bakker, A. R. Bowie, K. Buesseler, and H. Chang (2000), A mesoscale phytoplankton bloom in the polar Southern Ocean stimulated by iron fertilization, *Nature*, *407*(6805), 695–702.

Caldeira, K., and M. E. Wickett (2003), Oceanography: Anthropogenic carbon and ocean pH, *Nature*, *425*(6956), 365–365.

Cai, W. J., et al. (2010), Decrease in the CO_2 uptake capacity in an ice-free Arctic Ocean basin, *Science*, *329*(5991), 556.

Chang, C. H., N. C. Johnson, and N. Cassar (2014), Neural network-based estimates of Southern Ocean net community production from in situ ΔO_2/Ar and satellite observation: A methodological study, *Biogeosciences*, *11*(12), 3279–3297.

Charlson, R. J., J. E. Lovelock, M. O. Andreaei, and S. G. Warren (1987), Oceanic phytoplankton, atmospheric sulphur, cloud albedo and climate, *Nature*, *326*, 655–661.

Chen, L., Z. Gao, X. Yang, and W. Wang (2004), Comparison of air-sea fluxes of CO_2 in the Southern Ocean and the western Arctic Ocean, *Acta Oceanol. Sin.*, *23*(4), 647–653.

Chu, S., S. Elliott, and M. E. Maltrud (2003), Global eddy permitting simulations of surface ocean nitrogen, iron, sulfur cycling, *Chemosphere*, *50*, 223–235.

Clément, D. B. M., M. Gurvan, A. S. Fischer, L. Alban, and I. Daniele (2004), Mixed layer depth over the global ocean: An examination of profile data and a profile-based climatology, *J. Geophys. Res.*, *109*, C12003, doi:10.1029/2004JC002378.

Curran, M. A. J., and G. B. Jones (2000), Dimethyl sulfide in the Southern Ocean: Seasonality and flux, *J. Geophys. Res.*, *105*, 20,451–20,459, doi:10.1029/2000JD900176.

Curran, M. A. J., G. B. Jones, and H. Burton (1998), Spatial distribution of dimethylsulfide and dimethylsulfoniopropionate in the Australasian sector of the Southern Ocean, *J. Geophys. Res.*, *103*, 16,677–16,689, doi:10.1029/97JD03453.

Dunne, J. P., R. A. Armstrong, A. Gnanadesikan, and J. L. Sarmiento (2005), Empirical and mechanistic models for the particle export ratio, *Global Biogeochem. Cycles*, *19*, GB4026, doi:10.1029/2004GB002390.

Fogelqvist, E. (1991), Dimethylsulphide (DMS) in the Weddell Sea surface and bottom water, *Mar. Chem.*, *35*(1–4), 169–177.

Gao, Z., L. Chen, and G. Yuan (2008), Air-sea carbon fluxes and their controlling factors in the Prydz Bay in the Antarctic, *Acta Oceanol. Sin.*, *27*(3), 136–146.

Gao, Z., L. Chen, H. Sun, B. Chen, and W.-J. Cai (2012), Distributions and air–sea fluxes of carbon dioxide in the Western Arctic Ocean, *Deep Sea Res., Part II*, *81–84*, 46–52.

Inomata, Y., M. Hayashi, K. Osada, and Y. Iwasaka (2006), Spatial distributions of volatile sulfur compounds in surface seawater and overlying atmosphere in the northwestern Pacific Ocean, eastern Indian Ocean, and Southern Ocean, *Global Biogeochem. Cycles*, *20*, GB2022, doi:10.1029/2005GB002518.

Ishii, M., H. Y. Inoue, and H. Matsueda (2002), Net community production in the marginal ice zone and its importance for the variability of the oceanic pCO_2 in the Southern Ocean south of Australia, *Deep Sea Res., Part II*, *49*(9–10), 1691–1706.

Kameyama, S., et al. (2013), Strong relationship between dimethyl sulfide and net community production in the western subarctic Pacific, *Geophys. Res. Lett.*, *40*, 3986–3990, doi:10.1002/grl.50654.

Kameyama, S., S. Yoshida, H. Tanimoto, S. Inomata, K. Suzuki, and H. Yoshikawa-Inoue (2014), High-resolution observations of dissolved isoprene in surface seawater in the Southern Ocean during austral summer 2010–2011, *J. Oceanogr.*, *70*(3), 225–239.

Kettle, A., et al. (1999), A global database of sea surface dimethylsulfide (DMS) measurements and a procedure to predict sea surface DMS as a function of latitude, longitude, and month, *Global Biogeochem. Cycles*, *13*, 399–444, doi:10.1029/1999GB900004.

Kettle, A. J., and M. O. Andreae (2000), Flux of dimethylsulfide from the oceans: A comparison of updated data sets and flux models, *J. Geophys. Res.*, *106*, 26,793–26,808, doi:10.1029/2000JD900252.

Kiene, R. P., D. J. Kieber, D. Slezak, D. A. Toole, D. A. del Valle, J. Bisgrove, J. Brinkley, and A. Rellinger (2007), Distribution and cycling of dimethylsulfide, dimethylsulfoniopropionate, and dimethylsulfoxide during spring and early summer in the Southern Ocean south of New Zealand, *Aquat. Sci.*, *69*(3), 305–319.

Lana, A., T. Bell, R. Simó, S. M. Vallina, J. Ballabrera-Poy, A. Kettle, J. Dachs, L. Bopp, E. Saltzman, and J. Stefels (2011), An updated climatology of surface dimethlysulfide concentrations and emission fluxes in the global ocean, *Global Biogeochem. Cycles*, *25*, GB1004, doi:10.1029/2010GB003850.

Landschützer, P., et al. (2015), The reinvigoration of the Southern Ocean carbon sink, *Science*, *349*(6253), 1221–1224.

Laws, E. A., E. D'Sa, and P. Naik (2011), Simple equations to estimate ratios of new or export production to total production from satellite-derived estimates of sea surface temperature and primary production, *Limnol. Oceanogr. Methods*, *9*(12), 593–601.

Levasseur, M. (2011), Ocean science: If Gaia could talk, *Nat. Geosci.*, *4*(6), 351–352.

Llido, J., V. Garçon, J. R. E. Lutjeharms, and J. Sudre (2005), Event-scale blooms drive enhanced primary productivity at the subtropical convergence, *Geophys. Res. Lett.*, *321*, 291–310, doi:10.1029/2005GL022880.

Lizotte, M., M. Levasseur, S. Michaud, M. G. Scarratt, A. Merzouk, M. Gosselin, J. Pommier, R. B. Rivkin, and R. P. Kiene (2012), Macroscale patterns of the biological cycling of dimethylsulfoniopropionate (DMSP) and dimethylsulfide (DMS) in the Northwest Atlantic, *Biogeochemistry*, *110*(1–3), 183–200.

Lizotte, M. P. (2001), The contributions of sea ice algae to Antarctic marine primary production, *Am. Zool.*, *41*(1), 57–73.

Marandino, C. A., S. Tegtmeier, K. Krüger, C. Zindler, E. L. Atlas, F. Moore, and H. W. Bange (2013), Dimethylsulphide (DMS) emissions from the west Pacific Ocean: A potential marine source for the stratospheric sulphur, *Atmos. Chem. Phys.*, *13*(16), 8427–8437.

Metzl, N., C. Beauverger, C. Brunet, C. Goyet, and A. Poisson (1991), Surface water carbon dioxide in the southwest Indian sector of the Southern Ocean: A highly variable CO_2 source/sink region in summer, *Mar. Chem.*, *35*(1), 85–95.

Metzl, N., B. Tilbrook, and A. Poisson (1999), The annual fCO_2 cycle and the air-sea CO_2 flux in the sub-Antarctic Ocean, *Tellus B*, *51*(4), 849–861.

Morel, A., and J.-F. Berthon (1989), Surface pigments, algal biomass profiles, and potential production of the euphotic layer: Relationships reinvestigated in view of remote-sensing applications, *Limnol. Oceanogr.*, *34*(8), 1545–1562.

Orsi, A. H., H. T. Whitworth III, and W. D. Nowlin Jr. (1995), On the meridional extent and fronts of the Antarctic Circumpolar Current, *Deep Sea Res., Part I*, *42*(5), 641–673.

Park, K.-T., et al. (2014), Direct linkage between dimethyl sulfide production and microzooplankton grazing, resulting from prey composition change under high partial pressure of carbon dioxide conditions, *Environ. Sci. Technol.*, *48*(9), 4750–4756.

Park, M. G., S. R. Yang, S.-H. Kang, K. H. Chung, and J. H. Shim (1999), Phytoplankton biomass and primary production in the marginal ice zone of the northwestern Weddell Sea during austral summer, *Polar Biol.*, *21*(4), 251–261.

Poisson, A., N. Metzl, C. Brunet, B. Schauer, B. Bres, D. Ruiz-Pino, and F. Louanchi (1993), Variability of sources and sinks of CO2 in the western Indian and Southern Oceans during the year 1991, *J. Geophys. Res.*, *98*, 22,759–22,778, doi:10.1029/93JC02501.

Sabine, C. L., R. A. Feely, N. Gruber, R. M. Key, K. Lee, J. L. Bullister, R. Wanninkhof, C. S. Wong, B. Tilbrook, and F. J. Millero (2004), The oceanic sink for anthropogenic CO_2, *Science*, *305*(5682), 367–371.

Simó, R., and J. Dachs (2002), Global ocean emission of dimethylsulfide predicted from biogeophysical data, *Global Biogeochem. Cycles*, *16*(4), 1078, doi:10.1029/2001GB001829.

Simó, R., and C. Pedros-Alio (1999), Role of vertical mixing in controlling the oceanic production of dimethyl sulphide, *Nature*, *402*(6760), 396–399.

Six, K. D., S. Kloster, T. Ilyina, and S. D. Archer (2013), Global warming amplified by reduced sulphur fluxes as a result of ocean acidification, *Nat. Clim. Change*, *3*(11), 975–978.

Smith, W., and D. M. Nelson (1990), Phytoplankton growth and new production in the Weddell Sea marginal ice zone in the austral spring and autumn, *Limnol. Oceanogr.*, *35*(4), 809–821.

Smith, W. O., and J. C. Comiso (2008), Influence of sea ice on primary production in the Southern Ocean: A satellite perspective, *J. Geophys. Res.*, *113*, C05S93, doi:10.1029/2007JC004251.

Spreen, G., L. Kaleschke, and G. Heygster (2008), Sea ice remote sensing using AMSR-E 89-GHz channels, *J. Geophys. Res.*, *113*, C02S03, doi:10.1029/2005JC003384.

Staubes, R., and H. W. Georgii (1993), Biogenic sulfur compounds in seawater and the atmosphere of the Antarctic region, *Tellus B*, *45*(2), 127–137.

Stefels, J., M. Steinke, S. Turner, G. Malin, and S. Belviso (2007), Environmental constraints on the production and removal of the climatically active gas dimethylsulphide (DMS) and implications for ecosystem modelling, *Biogeochemistry*, *83*(1), 245–275.

Stoll, M. H. C., H. Thomas, H. J. W. De Baar, I. Zondervan, E. De Jong, U. V. Bathmann, and E. Fahrbach (2002), Biological versus physical processes as drivers of large oscillations of the air-sea CO_2 flux in the Antarctic marginal ice zone during summer, *Deep Sea Res., Part I*, *49*(9), 1651–1667.

Takahashi, T., J. Olafsson, J. G. Goddard, D. W. Chipman, and S. Sutherland (1993), Seasonal variation of CO_2 and nutrients in the high-latitude surface oceans: A comparative study, *Global Biogeochem. Cycles*, *7*, 843–878, doi:10.1029/93GB02263.

Takahashi, T., S. C. Sutherland, C. Sweeney, A. Poisson, N. Metzl, B. Tilbrook, N. Bates, R. Wanninkhof, R. A. Feely, and C. Sabine (2002), Global sea-air CO_2 flux based on climatological surface ocean pCO_2, and seasonal biological and temperature effects, *Deep Sea Res., Part II*, *49*, 1601–1622.

Taylor, M. H., M. Losch, and A. Bracher (2013), On the drivers of phytoplankton blooms in the Antarctic marginal ice zone: A modeling approach, *J. Geophys. Res. Oceans*, *118*, 63–75, doi:10.1029/2012JC008418.

Tortell, P., C. Gueguen, M. Long, C. Payne, P. Lee, and G. DiTullio (2011), Spatial variability and temporal dynamics of surface water pCO_2, ΔO_2/Ar and dimethylsulfide in the Ross Sea, Antarctica, *Deep Sea Res., Part I*, *58*, 241–259.

Tortell, P. D., and M. C. Long (2009), Spatial and temporal variability of biogenic gases during the Southern Ocean spring bloom, *Geophys. Res. Lett.*, *36*, L01603, doi:10.1029/2008GL035819.

Tortell, P. D., M. C. Long, C. D. Payne, A. C. Alderkamp, P. Dutrieux, and K. R. Arrigo (2012), Spatial distribution of pCO_2, ΔO_2/ Ar and dimethylsulfide (DMS) in polynya waters and the sea ice zone of the Amundsen Sea, Antarctica, *Deep Sea Res., Part II*, *71-76*, 77–93.

Trevena, A., and G. Jones (2012), DMS flux over the Antarctic sea ice zone, *Mar. Chem.*, *134–135*, 47–58.

Trevena, A. J., and G. B. Jones (2006), Dimethylsulphide and dimethylsulphoniopropionate in Antarctic sea ice and their release during sea ice melting, *Mar. Chem.*, *98*(2), 210–222.

Turner, S., P. Nightingale, W. Broadgate, and P. Liss (1995), The distribution of dimethyl sulphide and dimethylsulphoniopropionate in Antarctic waters and sea ice, *Deep Sea Res., Part II*, *42*(4), 1059–1080.

Vallina, S. M., and R. Simó (2007), Strong relationship between DMS and the solar radiation dose over the global surface ocean, *Science*, *315*(5811), 506–508.

Vila-Costa, M., J. M. Rinta-Kanto, R. S. Poretsky, S. Sun, R. P. Kiene, and M. A. Moran (2014), Microbial controls on DMSP degradation and DMS formation in the Sargasso Sea, *Biogeochemistry*, *120*(1), 295–305.

Vogt, M., and P. Liss (2009), Dimethylsulfide and climate, *Geophys. Monogr. Ser.*, *187*, 197–232.

Wang, S., D. Bailey, K. Lindsay, J. K. Moore, and M. Holland (2014), Impact of sea ice on the marine iron cycle and phytoplankton productivity, *Biogeosciences*, *11*(17), 4713–4731.

Wanninkhof, R. (1992), Relationship between wind speed and gas exchange, *J. Geophys. Res.*, *97*, 7373–7382, doi:10.1029/92JC00188.

Watanabe, Y. W., H. Yoshinari, A. Sakamoto, Y. Nakano, N. Kasamatsu, T. Midorikawa, and T. Ono (2007), Reconstruction of sea surface dimethylsulfide in the north pacific during 1970s to 2000s, *Mar. Chem.*, *103*(3–4), 347–358.

Yang, G. P., H. H. Zhang, L. M. Zhou, and J. Yang (2011), Temporal and spatial variations of dimethylsulfide (DMS) and dimethylsulfoniopropionate (DMSP) in the East China Sea and the Yellow Sea, *Cont. Shelf. Re.*, *31*(13), 1325–1335.

Yang, G.-P., G.-C. Zhuang, H.-H. Zhang, Y. Dong, and J. Yang (2012), Distribution of dimethylsulfide and dimethylsulfoniopropionate in the Yellow Sea and the East China Sea during spring: Spatio-temporal variability and controlling factors, *Mar. Chem.*, *138*, 21–31.

Zhang, M., and L. Chen (2015), Continuous underway measurements of dimethyl sulfide in seawater by purge and trap gas chromatography coupled with pulsed flame photometric detection, *Mar. Chem.*, *174*, 67–72.

Zhang, M., L. Chen, G. Xu, Q. Lin, and M. Liang (2015), Linking phytoplankton activity in polynya and sulfur aerosols at Zhongshan station, East Antarctica, *J. Atmos. Sci.*, *72*(12), 4629–4642.

Zindler, C., A. Bracher, C. A. Marandino, B. Taylor, E. Torrecilla, A. Kock, and H. W. Bange (2013), Sulphur compounds, methane, and phytoplankton: Interactions along a north–south transit in the western Pacific Ocean, *Biogeosciences*, *10*(5), 3297–3311, doi:10.5194/bg-10-3297-2013.